Tunneling Nanotubes are Novel Cellular Structures That Communicate Signals Between Trabecular Meshwork Cells

Kate E. Keller, John M. Bradley, Ying Ying Sun, Yong-Feng Yang, and Ted S. Acott

Casey Eye Institute, Oregon Health & Science University, Portland, Oregon, United States

Correspondence: Kate E. Keller, Casey Eye Institute, Oregon Health & Science University, 3181 SW Sam Jackson Park Road, Portland, OR 97239, USA; gregorka@ohsu.edu.

PURPOSE. The actin cytoskeleton of trabecular meshwork (TM) cells plays a role in regulating aqueous humor outflow. Many studies have investigated stress fibers, but F-actin also assembles into other supramolecular structures including filopodia. Recently, specialized filopodia called tunneling nanotubes (TNTs) have been described, which communicate molecular signals and organelles directly between cells. Here, we investigate TNT formation by TM cells.

METHODS. Human TM cells were labeled separately with the fluorescent dyes, DiO and DiD, or with mitochondrial dye. Fixed or live TM cells were imaged using confocal microscopy. Image analysis software was used to track fluorescent vesicles and count the number and length of filopodia. The number of fluorescently labeled vesicles transferred between cells was counted in response to specific inhibitors of the actin cytoskeleton. Human TM tissue was stained with phalloidin.

RESULTS. Live-cell confocal imaging of cultured TM cells showed transfer of fluorescently labeled vesicles and mitochondria via TNTs. In TM tissue, a long (160 μm) actin-rich cell process bridged an intertrabecular space and did not adhere to the substratum. Treatment of TM cells with CK-666, an Arp2/3 inhibitor, significantly decreased the number and length of filopodia, decreased transfer of fluorescently labeled vesicles and induced thick stress fibers compared to vehicle control. Conversely, inhibiting stress fibers using Y27632 increased transfer of vesicles and induced long cell processes.

CONCLUSIONS. Identification of TNTs provides a means by which TM cells can directly communicate with each other over long distances. This may be particularly important to overcome limitations of diffusion-based signaling in the aqueous humor fluid environment.

Keywords: trabecular meshwork, tunneling nanotubes, actin cytoskeleton, live cell imaging

Trabecular meshwork (TM) cells communicate by secreting soluble signaling factors or encapsulating signals in small lipid-derived nanovesicles called exosomes.[1] Soluble signals and exosomes diffuse through the extracellular space and positively or negatively regulate neighboring TM cell function.[2–5] However, in the anterior chamber of the eye, aqueous humor (AH) fluid is a major barrier to diffusional-based signaling. All secreted signals are continually diluted and washed away by the continual flow of AH into Schlemm's canal. Thus, it is unlikely that signals can survive extracellularly at high enough concentrations to signal more than one or two cell diameters. Moreover, because AH flow is unidirectional, TM cells deep in the outflow pathway, such as those in the juxtacanalicular (JCT) region (Fig. 1A), cannot use a diffusional-based mechanism to communicate with cells in the corneoscleral or uveal meshwork. Furthermore, signals in TM tissue also appear to travel relatively long distances. This was demonstrated in a study utilizing argon laser trabeculoplasty, a surgical technique used to reduce IOP in glaucoma patients.[6] Laser spots placed on the TM beams stimulated cell division in the insert region, a putative TM stem cell niche >200 μm away (Fig. 1A).[7] The insert region is not bathed in AH so signals cannot be transported there in fluid. Thus, it remains unclear how signals could be transferred long distances from the laser sites to the insert region. It is possible that signals could be transferred via a signal relay or "bucket brigade" where signaling molecules undergo repeated rounds of secretion, receptor-mediated endocytosis on a recipient cell, trafficking through the intracellular endocytic pathway, and exocytosis.[8] However, green fluorescent protein (GFP)-tagged decapentaplegic was only propagated up to 80 μm in highly compliant embryonic tissue.[9] This distance is insufficient to bridge the space between the laser sites and the insert region. Thus, additional nondiffusion-based communication mechanisms must exist to transfer signals between cells in different regions of the TM in situ.

Actin monomers rapidly and reversibly polymerize to form microfilaments, which are organized into higher ordered structures such as stress fibers, lamellipodia and filopodia.[10,11] The assembly of these supramolecular structures are governed by the small GTPases RhoA, Rac1, and cdc42, respectively.[12] Inhibition of the Rho-ROCK signaling pathway increases aqueous outflow through the TM.[13–18] Stress fibers are the predominant F-actin structure in cultured TM cells, but actin stress fibers are not a predominant structure in TM tissue in situ.[19] Thus, the mechanistic details of how Rho kinase inhibition leads to greater outflow facility remain unclear. Furthermore, although stress fiber formation has been studied extensively in the TM, the relative contribution of the other F-
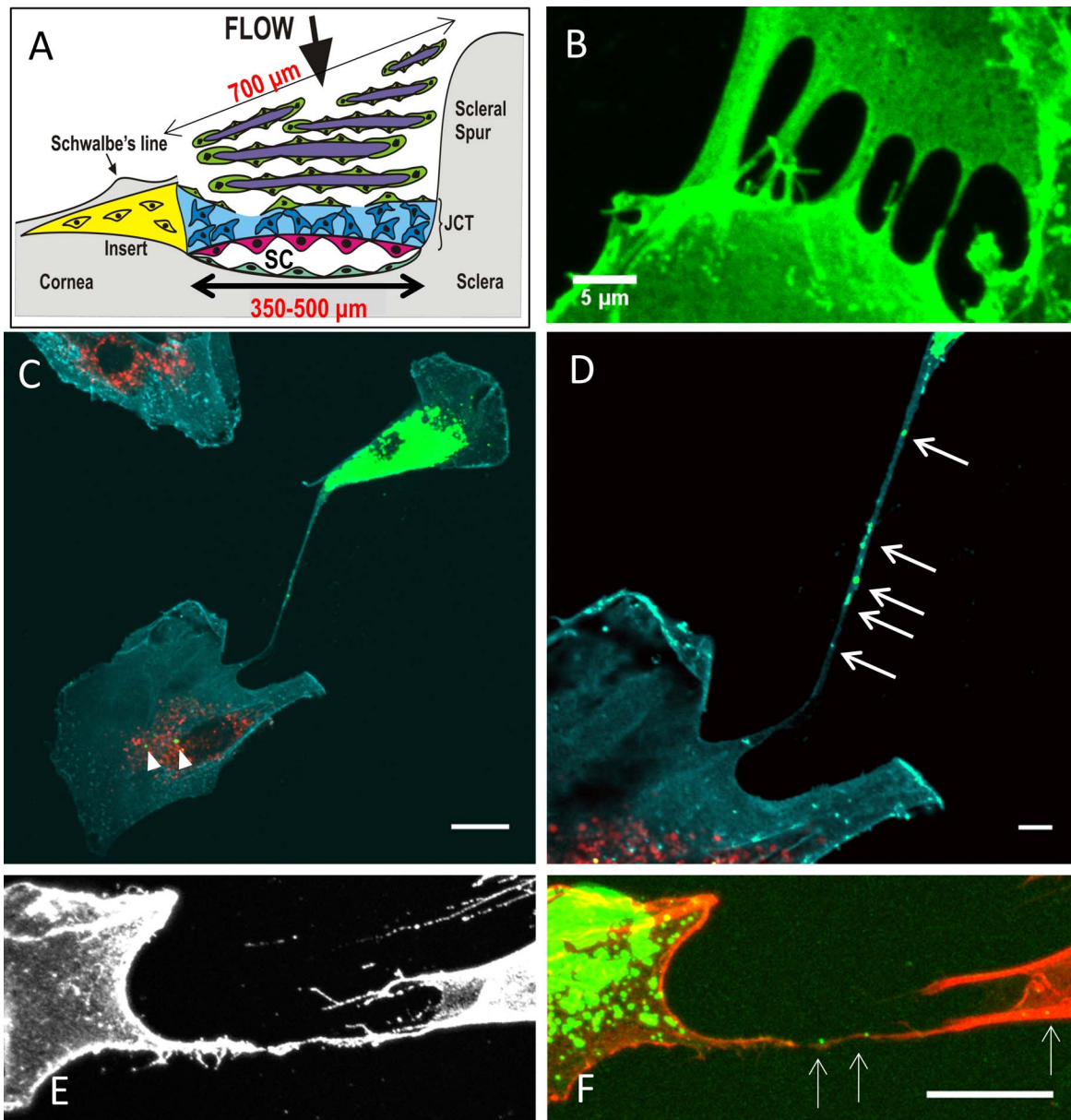
FIGURE 1. (A) Schematic of a cross-section of the TM, with the regions and approximate dimensions of the tissue indicated. TM cells (*green*); corneoscleral beams (*purple*); the JCT region (*blue*); the inner wall cells of Schlemm's canal (*pink*); the putative stem cell insert region (*yellow*); and Schlemm's canal. (B) TM cells immunostained with CD44 to label the cell membrane. Filopodia from neighboring cells appear to touch and fuse to form a tube. *Scale bar*: 5 μm. (C) In coculture experiments, DiO-labeled vesicles (*green*) were present in a DiD-labeled (*red*) cell (*arrowheads*). *Cyan*: CD44; *scale bar*: 20 μm. (D) At higher magnification, DiO-labeled vesicles are clearly visible (*arrows*) within a long cell process connecting the two cells. *Scale bar*: 5 μm. (E) CD44 immunostaining (*gray*) of a TNT connecting two TM cells. (F) DiO-labeled vesicles (*green; arrows*) are clearly visible within the SiR-actin-labeled cell process (*red*). *Scale bar*: 20 μm.

actin supramolecular assemblies to TM cell function has been mostly overlooked.

Filopodia are thin, finger-like projections that contain tight bundles of F-actin.[11] A newly identified class of specialized filopodia is called tunneling nanotubes (TNTs).[20-22] TNTs form tubular conduits to directly transfer molecular information and organelles between cells and are a novel mechanism of cellular communication. Cargoes transported include endosomes, lysosomes, mitochondria, viruses, prions and miRNAs.[20,23-26] TNTs can form between homotypic cells or they can connect different cell types such as stem cells and endothelial cells.[24,25,27] Several reports have detected TNT formation by other ocular cell types including dendritic cells and hemato-

poietic stem progenitor cells in the mouse cornea and cultured human retinal pigment epithelial cells.[28-30] In this study, we investigated whether TM cells could form TNTs to directly communicate signals over long distances.

METHODS

Confocal Microscopy of Fixed Cells and Tissue

Primary TM cells were isolated from human cadaver eyes (Lions VisionGift, Portland, OR, USA) using established methods.[31] The use of human cadaver tissue was approved by Oregon Health & Science University Institutional Review

Board and experiments were conducted in accordance with the tenets of the Declaration of Helsinki. At least five biological replicates were used from donors ranging from 3 to 47 years old. All HTM cell strains induced myocilin by Western immunoblotting after 2 weeks of dexamethasone treatment (data not shown). Once confluent, a flask of TM cells was trypsinized, split into two tubes and separately labeled with Vybrant DiD dye (647 nm) or Vybrant DiO dye (488 nm; Thermo Fisher Scientific, Waltham, MA, USA). In other experiments, cells were labeled with the mitochondrial dye, (594 nm MitoTracker Red CMXRos; Thermo Fisher Scientific), and DiO. Fluorescently labeled cells were mixed 1:1 and plated at 1×10^5 cells per well on collagen type I-coated BioFlex 6-well plates (FlexCell International Corp., Burlington, NC, USA). After overnight incubation, cells were fixed and immuno-stained with rat monoclonal anti-CD44, clone IM-7 (Stem Cell Technologies, Vancouver, BC), which was detected with an AlexaFluor 594-conjugated goat anti-rat secondary antibody (Thermo Fisher Scientific). In some experiments, TM cells were labeled with 0.1 µM SiR-actin (Spirochrome, Cytoskeleton, Inc., Denver, CO, USA) with 10 µM verapamil during the overnight incubation. TM cells were then imaged using a confocal microscope (Fluoview FV1000; Olympus, Waltham, MA, USA). Images were stacked and processed using open-source FIJI software (http://fiji.sc/Fiji, in the public domain).

Live-Cell Imaging

For live-cell imaging, cells were plated in 2-well slides (µ-slides; Ibidi, Madison, WI, USA) and imaged using a widefield system (Deltavision Core DV; GE Healthcare Life Sciences, Pittsburgh, PA, USA) at 37°C in a humidified environment with 5% CO_2. This system consists of an inverted microscope (IX71; Olympus) with a ×60 Plan-Apochromat objective (1.42 NA) and a camera (Coolsnap ES2 HQ; Nikon Corp., Tokyo, Japan). Images were captured every 2 minutes for a total of 4 hours on 3 z-planes and fluorescence was detected in the GFP (488 nm) and Cy5 (647 nm) channels. A differential interference contrast (DIC) image was captured at the central z-plane at each time point. Following acquisition, z-planes were stacked and the images were animated into a time-lapse movie at 12 frames per second. For some movies, the 488-nm channel was overlaid onto the DIC image. In addition, image analysis software (Imaris; Bitplane, Concord, MA, USA) was used to analyze the movies frame by frame and a dot was manually placed on DiO-labeled vesicles in each frame. The software then added a "dragon tail" to denote from where the vesicles had come.

Staining of Human TM Tissue

To visualize F-actin in TM tissue, human cadaver anterior segments ($n = 3$) were immersion-fixed in 4% paraformalde-hyde and frontal sections were cut perpendicular to the ocular surface.[17] After a brief permeabilization with 0.02% Tween-20, tissue pieces were incubated AlexaFluor 488–conjugated phalloidin (Thermo Fisher Scientific). Tissues were immersed in gold-mounting medium (ProLong; Thermo Fisher Scientific) containing DAPI and imaged using the confocal microscope (Olympus) with a ×60 Plan-Apochromat objective (1.42 NA). At least three tissue pieces per eye were examined. For the image shown, eighteen 0.2-µm z-slices were acquired and then stacked using FIJI software.

Actin Inhibitor Experiments

TM cells were treated with 100 µM CK-666 ($n = 23$ cells) or DMSO vehicle control ($n = 27$ cells). The number and length of filopodia on the surface of TM cells was measured using the filaments module of the image analysis software (Bitplane). Data from three biological replicates were combined and a box-and-whisker plot was generated to show the median and the upper and lower quartiles. Significance ($P < 0.05$) was determined from the mean values (gray diamonds) using ANOVA with Bonferroni post-hoc correction.

To quantitate the number of vesicles transferred, cells were fluorescently labeled as above and allowed to adhere for 2 hours. The following actin inhibitors were added: 100 µM CK-666,[32] 10 µM ML141, 5 µM Y27632, 10 µM wiskostatin, 0.78 µM cytochalasin D, 0.1 µM latrunculin B, or 0.04% DMSO vehicle control (Sigma-Aldrich Corp., Saint Louis, MO, USA). Cells were incubated for a further 24 hours and then fixed and immunostained with CD44 antibodies as above. Confocal images were acquired and each fluorescent channel was analyzed separately. The number of TM cells containing at least five vesicles of the opposite color was counted in each image. Vesicles were not counted if they were not visible within the boundaries of the CD44-stained cell membrane. The number of cells containing "transferred" vesicles was made a percentage of total cell number. This was repeated in >6 independent experiments, using HTM cells derived from five biological replicates. A box-and-whisker plot was generated as above. Outliers were defined as those lying outside of ×1.5 interquartile range, as defined by Tukey, and were omitted from the calculations (outliers: $n = 2$ for control; $n = 1$ for Wiskostatin; $n = 0$ for all other treatments). Significance ($P < 0.05$) was determined from the mean values (blue diamonds) using ANOVA with Bonferroni post-hoc correction.

Visualizing Actin Dynamics in Live TM Cells

To visualize actin dynamics live, TM cells were plated in a 4-well slide (Ibidi) and labeled overnight with 0.1 µM SiR-actin with 10 µM verapamil. The following day, medium was replaced and inhibitors were added (100 µM CK-666; 5 µM Y27632; 0.04% DMSO vehicle control) for 3 hours prior to imaging on a widefield system (GE Healthcare Life Sciences). Images were acquired in the Cy5 (647 nm) channel every minute for a total of 30 minutes on 3 z-planes. Captured images were deconvolved using commercial software (GE Healthcare Life Sciences), stacked and movies were made at 3 frames per second.

RESULTS

To investigate TNT formation by TM cells, primary cultures were immunostained with the cell membrane protein, CD44. Filopodia extended from adjacent cells to touch their tips (Fig. 1B). Some appeared to have fused suggesting the formation of TNTs so we fluorescently labeled cell organelles to see if we could detect cargo within the tubular conduit. TM cells were separately labeled with the fluorescent dyes, DiO or DiD, and were mixed 1:1 at low cell density (1×10^5 cells/well). A long filopodia (~240 µm) extended between a DiO-labeled cell (green) and a DiD-stained cell (red; Fig. 1C). At higher magnification, DiO-stained vesicles (green) were clearly observed in the connecting tube and the cytosol of a DiD-stained cell (red; Fig. 1D). No DiD-labeled vesicles were present in this DiO cell suggesting unidirectional transfer.[20] To demonstrate that F-actin was a component of TNTs, F-actin of TM cells was labeled with SiR-actin. Again, CD44 was used to label the cell surface (Fig. 1E), while DiO-labeled vesicles (green; arrows) were clearly observed traveling along the SiR-actin-labeled TNT (red; Fig. 1F).

Studies of other cell types have demonstrated that mitochondria are transferred via TNTs.[24,27] Therefore, we

tested whether mitochondria were transferred in TM cells. TM cells were separately labeled with DiO (green) or a mitochondrial fluorescent stain (red; Thermo Fisher Scientific). After mixing and overnight incubation as above, mitochondria (red) were clearly visible in a DiO-labeled cell (green; Fig. 2A) and in a TNT connecting two cells (arrows; Fig. 2B). Thus, TM cells appear to transfer mitochondria via TNTs.

To provide further support for TNT formation by TM cells, live-cell confocal microscopy was performed. Still frames are shown in Figure 3. The top panels (Figs. 3A, 3B) show DiO-labeled cells (green) overlaid onto a DIC image at the first (0 minutes) and last (240 minutes) frames of the movie, respectively. The cell at the top right is labeled with mitochondrial dye (red, inset; Thermo Fisher Scientific). At the start of the movie, the red cell already contained some green vesicles due to transfer prior to imaging. The movies demonstrate that the TM cell membrane is highly dynamic and multiple filopodia are formed at the cell surface (Supplementary Fig. S1). One of these filopodia formed a "tube" (arrows) and DiO-labeled vesicles (green) are transferred to the cell labeled with mitochondrial dye (Thermo Fisher Scientific) through the conduit (Figs. 3C, 3D). Image analysis software (Bitplane) was used to add "dragon tails" (cyan) to the vesicles to aid tracking of their movement (Figs. 3E–G). Four vesicles were calculated to be completely transferred via one TNT in 40 minutes.

Electron microscopy studies of the TM have described long cell processes extending between cells in the JCT region and cells residing on TM beams.[33–36] Here, frontal sections were labeled with AlexaFluor 488–phalloidin to investigate whether long actin-rich processes could be detected in human TM tissue in situ (Fig. 4). Confocal microscopy showed a long, actin-rich cell process bridging an intertrabecular space (~160 μm long; double-headed arrow). This cell process was not attached to the collagen beam running parallel to it, whereas other cell processes (arrowheads) appear tightly adhered to collagen beams (blue autofluorescence). The anchorage-independence and thin, long dimensions of these processes are similar to features described for TNTs.[22]

Next, we investigated the effects of specific actin inhibitors on TNT formation. The Arp2/3 inhibitor, CK-666, inhibits assembly of branched actin networks from which filopodia emanate.[32] Thus, CK-666 should reduce the number of filopodia/TNTs on TM cells. In this study, image analysis software (Bitplane) was used to count the number of filopodia on the surface of the TM cell membrane. Treatment with CK-666 significantly reduced the number of filopodia on the surface of TM cells (mean = 10.34 ± 0.65 filopodia/cell) compared to vehicle control cells (19.51 ± 1.06 filopodia/cell)($P < 0.001$; Fig. 5A). In addition, the length of filopodia was significantly shorter in CK-666–treated cells versus control cells (average length = 4.49 μm ± 0.225 vs. 8.35 μm ± 0.254; $P < 0.0001$; Fig. 5B).

We used additional specific inhibitors to measure the effects on vesicle transfer. ML141 inhibits the small GTPase, cdc42, while Wiskostatin inhibits N-WASP (Fig. 6A).[12] The Rho Kinase inhibitor, Y27632, was used to inhibit actin stress fibers, while cytochalasin D and Latrunculin B prevent assembly of F-actin into all supramolecular structures. DiO- and DiD-labeled TM cells were cocultured in the presence of the inhibitors and the number of cells containing vesicles of the opposite color ("transferred vesicles") was counted from confocal images. In DMSO vehicle control cultures, approximately $36.7\% \pm 2.9\%$ of cells contained transferred vesicles (Fig. 6B). Treatment with CK-666 significantly inhibited transfer with only approximately $27.1\% \pm 2.5\%$ of cells containing transferred vesicles ($P = 0.02$). Conversely, a significantly increased percentage of cells treated with the Rho kinase inhibitor, Y27632, contained
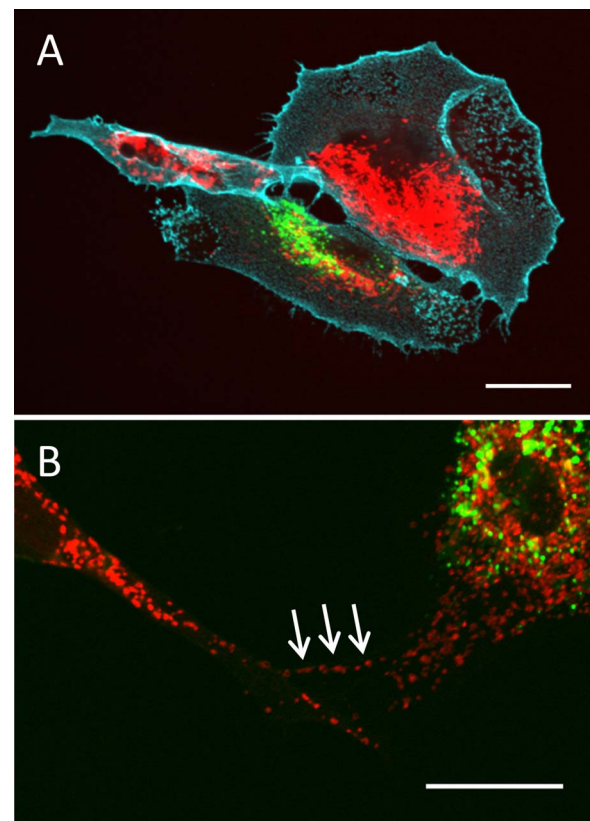
FIGURE 2. Transfer of mitochondria via TNTs. TM cells were labeled separately with dye (Thermo Fisher Scientific) to stain mitochondria (*red*) or the fluorescent dye, DiO (*green*), then mixed 1:1. (**A**) After overnight incubation, mitochondria (*red*) were observed in a DiO-labeled cell (*green*). *Cyan*: CD44 immunostaining. (**B**) A higher magnification image of labeled mitochondria (*red*; Thermo Fisher Scientific) in a DiO-labeled cell (*green*). *Arrows* point to mitochondria in a TNT. *Scale bar*: 20 μm.

transferred vesicles ($57.78\% \pm 4.1\%$; $P = 0.002$). ML141 treatment decreased transfer ($30.7\% \pm 2.2\%$), but not significantly, while Wiskostatin ($36.7\% \pm 2.8\%$) had no effect compared to vehicle controls. As expected, Latrunculin B and cytochalasin D significantly reduced vesicle transfer ($23.83\% \pm 2.2\%$ and $18.61 \pm 1.7\%$, respectively).

Representative confocal images of DMSO vehicle control, CK-666– and Y27632-treated TM cells demonstrate vesicle transfer between cells (Fig. 6C). In addition, CD44 immunostaining showed the profound effect of Y27632 on TM cell phenotype. Rho kinase inhibition induced very long thin cell processes which often extend the full length of the field of view and beyond. Fluorescently labeled vesicles were clearly visible in nearly all of these processes (Fig. 6C). Collectively, these results show that inhibition of stress fiber formation by Y27632 increased vesicle transfer, whereas inhibition of filopodia formation by CK-666 or preventing F-actin assembly (Latrunculin B or cytochalasin D) decreased transfer.

To further examine actin cytoskeletal dynamics, F-actin was stained with SiR-actin. Addition of this actin-label did not significantly affect TM cell morphology (data not shown). SiR-actin was used to label live TM cells and time-lapse movies were generated (Supplementary Fig. S2). Still images are shown in Figure 7. In DMSO-vehicle control TM cells (Figs. 7A–D), F-actin was assembled into stress fibers, cortical actin at the cell periphery and was present in punctate vesicles, which were predominantly located perinuclearly. Some actin bundles
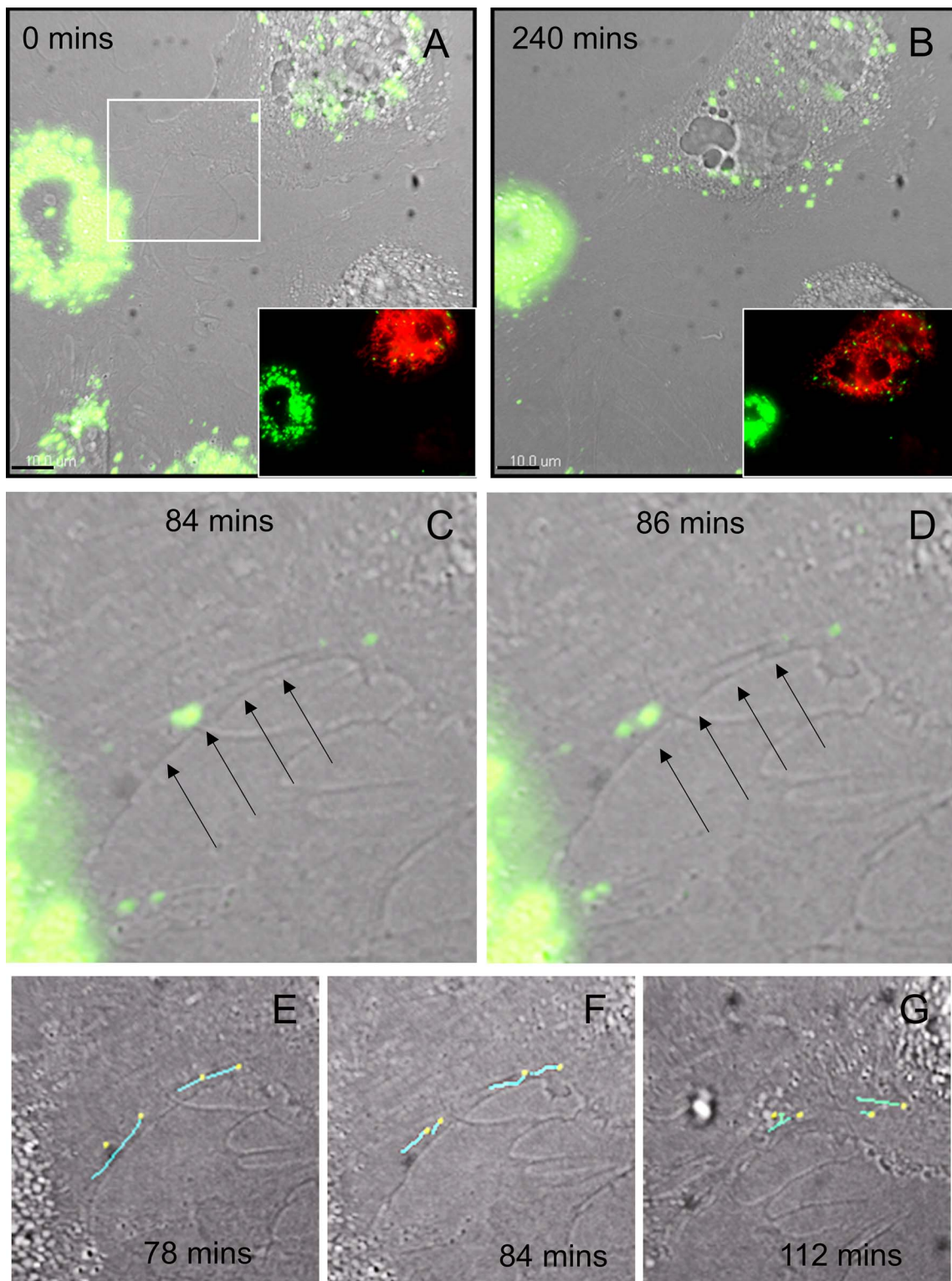
FIGURE 3. Still images from movies of live TM cells at 0 minutes (**A**) and at 240 minutes (**B**) with the DiO (*green*) channel overlaid onto a DIC image. The insets show the fluorescence channels to demonstrate that the cell at the top right is labeled with mitochondrial dye (*red*; Thermo Fisher Scientific). (**C, D**) The white boxed area in (**A**) is shown at 84 and 86 mins. A "tube" appears to be formed (*arrows*) between TM cells and green vesicles are clearly seen in the tubular interior. (**E–G**) Image analysis software (Bitplane) was used to add "dragon tails" to the vesicles to track their movement. For this, the 488-nm channel was analyzed frame-by-frame and a "dot" was manually placed on a vesicle in each frame. The software added a dragon tail (*cyan line*) to denote where the vesicles had come from. Dragon tails of 4 vesicles were overlaid onto the DIC images of 78, 84, and 112 minutes. *Scale bar*: 10 μm.
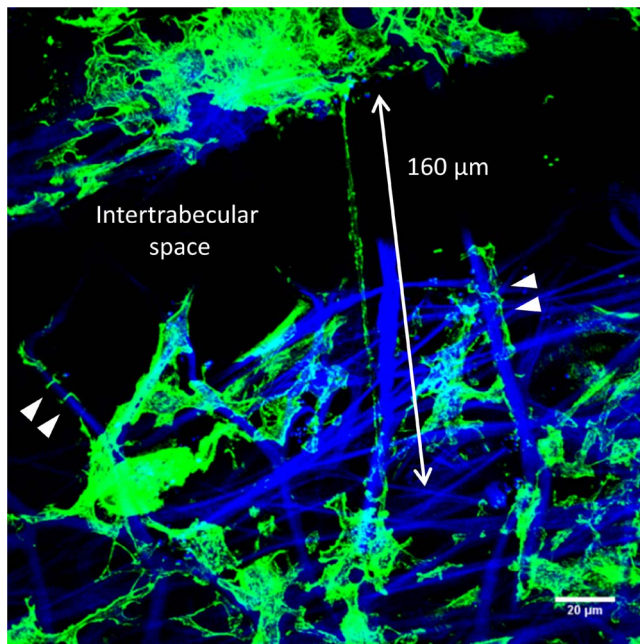
Figure 4. Frontal section of human TM tissue stained with AlexaFluor phalloidin (*green*) to label F-actin. A long, actin-rich cell process (approximately 160 μm) bridges an intertrabecular space between corneoscleral beams (*double-headed arrow*). Other F-actin-rich processes are tightly wrapped around the underlying collagen beams (*arrowheads*). *Blue*: DAPI staining and autofluorescence of collagenous TM beams. *Scale bar*: 20 μm.

Figure 5. Effect of CK-666 on filopodia number and length. (**A**) The average number of filopodia per cell and (**B**) the length of filopodia was quantitated using image analysis software (Bitplane) from TM cells treated with DMSO vehicle control ($n = 27$ cells, 496 filopodia counted) and CK-666 ($n = 23$ cells; 231 filopodia counted). Data are from three biological replicates. The gray diamond in each box is the mean value. * $P < 0.001$ by ANOVA with Bonferroni correction.

protruding from the cell surface are likely in filopodia (arrowhead). In CK-666–treated cells (Figs. 7E–H), the stress fibers and cortical actin fibers were thicker than in control cells. Moreover, there were fewer actin-positive punctate vesicles and they were distributed throughout the cell. One actin-positive protrusion retracted over the time frame (arrow) and there were few other cellular protrusions. In Y27632-treated cells (Figs. 7I–L), few stress fibers were present, as expected, but cortical actin remained. There was a major change in cell phenotype with many protrusions emanating from the cell surface, similar to CD44 immunostaining described above. The actin-rich punctate vesicles were highly dynamic and moved rapidly in the cells compared to control and CK-666–treated cells. They were distributed throughout the cell.

Discussion

In this study, we report the formation of TNTs by TM cells and demonstrated that fluorescently-labeled vesicles as well as mitochondria can be transported between TM cells. The TNTs extended approximately 240 μm between cells in culture and 160 μm in TM tissue. These lengths are similar to those described for TNTs formed by other cell types.[22] When compared to signaling ranges of other mechanisms, TNTs allow cellular communication over greater distances than diffusion-based signals (<80 μm),[9] but not as far as that of exosomes, which are secreted into biofluids and have a much farther range of signaling.[1,37] Moreover, TNTs can deliver signals directly to areas of the tissue not bathed in AH such as the putative TM stem cell niche and can communicate signals from JCT cells to corneoscleral meshwork TM cells, which is against AH outflow.
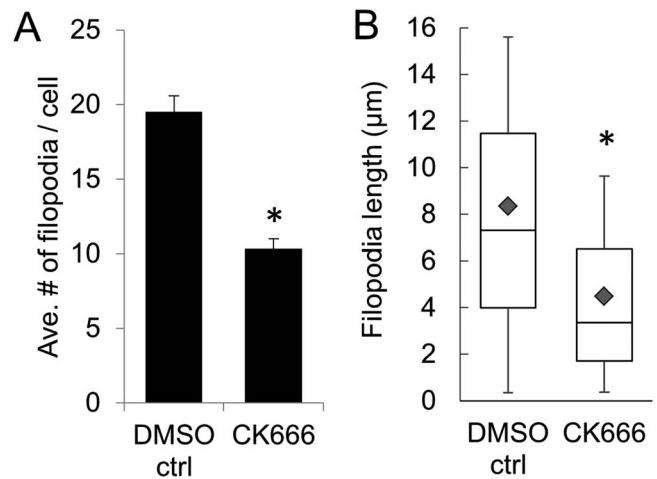
TNTs are transient structures and two models of TNT formation have emerged: the "cell dislodgement mechanism", where two adjacent cells fuse transiently and, as the cells move apart, a thin retraction tubule remains through which cargo can travel.[38,39] The other proposed model is an "actin driven protrusion mechanism." This is an active process whereby filopodia are extruded from two adjacent cells and when their tips touch, they undergo fusion to create a tunnel.[20,39] The movies shown here suggest that TNTs in TM cells are formed by an actin-driven mechanism because vesicle transfer was essentially complete before the cells retracted and moved away from each other. However, it remains possible that both mechanisms are used to form TNTs in TM cells. Furthermore, the mechanism utilized could be dependent on culture conditions. The TNT shown here was actively transporting vesicles for 40 minutes, which is similar to TNTs in other cell types where they endure from minutes to several hours.[22,40] Interestingly, the movie also shows formation of multiple filopodia at the TM cell surface, but only one of these transitioned into a TNT. What governs TNT formation is unclear. The unconventional myosin, myosin-10, appears to play a role in other cell types,[41,42] and in the case of electrically coupled TNTs, gap junction proteins may stabilize the contact at the tips of TNTs.[39] However, more studies are required to investigate which molecules are involved in TNT formation in TM cells.

In several of the experiments reported herein, CK-666 was used as an inhibitor. CK-666 stabilizes the Arp2/3 complex in an inactive state, which inhibits assembly of branched actin networks important for both lamellipodia and filopodia formation.[32] Lamellipodia are sheet-like actin-rich protrusions that are characteristic of motile cells.[11] Yet, the movies in this study show that TM cells are predominantly sedentary with few, if any, lamellipodia. Conversely, TM cells have many filopodia emanating from the underlying actin networks to protrude from the cell surface. Our results show that CK-666 significantly reduced the number of filopodia on the cell surface of treated TM cells as well as reduced the length of those filopodia that were present. Moreover, there was a significant reduction in the number of vesicles transferred.
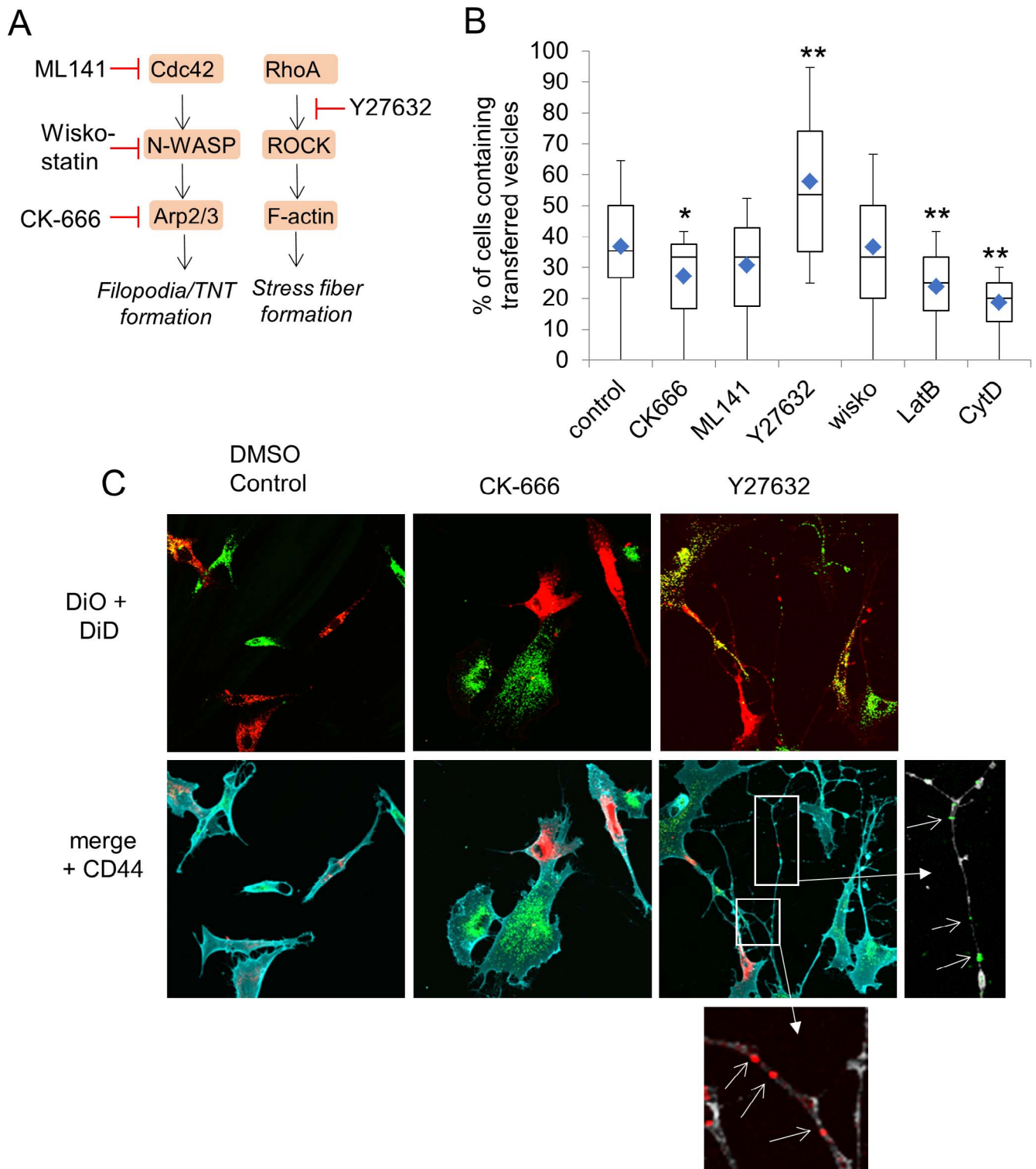
FIGURE 6. Effect of actin inhibitors on vesicle transfer. (A) Schematic of molecules involved in filopodia and stress fiber formation and their inhibitors. (B) The effects of inhibitors on vesicle transfer between TM cells. The percentage of TM cells containing vesicles of the opposite color were counted in confocal images of control (0.04% DMSO vehicle; $n = 58$ images; total no. of cells = 294) and TM cells treated with 100 μM CK-666 ($n = 53$ images; total no. of cells = 284);10 μM ML141 ($n = 66$ images; total no. of cells = 374); 5 μM Y27632 ($n = 35$ images; total no. of cells = 163); 10 μM wiskostatin ($n = 50$ images; total no. of cells = 259); 0.1 μM Latrunculin B ($n = 42$ images; total no. of cells = 227) and 0.78 μM cytochalasin D ($n = 25$ images; total no. of cells = 186). The blue diamond in each box is the mean value. Data are from five biological replicates. * $P = 0.02$ and ** $P < 0.002$ by ANOVA with Bonferroni correction. (C) Representative confocal images of control, CK-666– and Y27632-treated TM cells labeled with DiD (red); DiO (green); and CD44 (membrane; cyan) used for cell counts. Boxed regions show vesicles in long cell processes in Y27632-treated cells. Here, the CD44 immunostaining was made gray in order to highlight the fluorescently-colored vesicles. Scale bar: 20 μm.
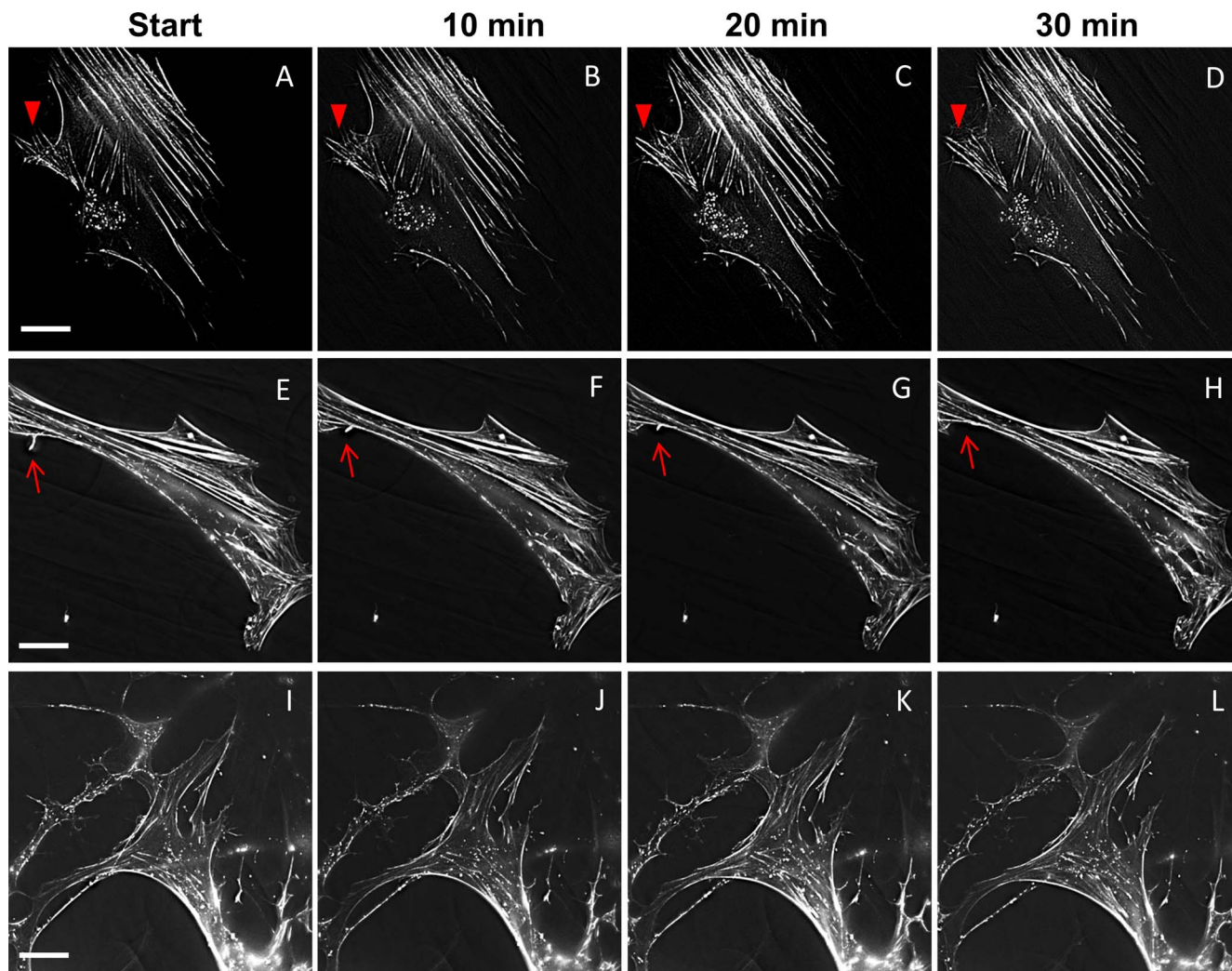
FIGURE 7. Actin dynamics in live human TM cells labeled with SiR-actin. Representative images of actin supramolecular structures from time-lapse movies at the start and after 10, 20, and 30 minutes in (**A–D**) DMSO control; (**E–H**) CK-666–; and (**I–L**) Y27632-treated TM cells. Arrowheads (**A–D**) and arrows (**E–H**) point to actin in cellular protrusions. *Scale bar*: 25 μm.

Collectively, these results suggest that Arp2/3 may play a role in TNT formation.

The Rho kinase inhibitor, Y27632, increased vesicle transfer via TNTs. CD44 immunostaining showed a dramatic change in cell phenotype with the formation of many long cell processes that contained fluorescently-labeled vesicles. Disassembly of F-actin stress fibers by Rho kinase inhibition may enrich the cellular pool of G-actin available for assembly into filopodia. This may in turn drive TNT formation and increase vesicular transfer by TNTs. Agents that disrupt all F-actin structures (cytochalasin D and latrunculin) decreased vesicle transfer, which was expected since TNTs contain actin. However, vesicle transfer was not completely eliminated. Low concentrations of inhibitors were used to prevent cell death during the experiment and thus F-actin assembly may not have been completely inhibited. Alternatively, it is possible that some vesicles were exchanged via endocytosis, phagocytosis or a non-actin based communication mechanism. Our data do not exclude communication by these mechanisms, but describe an additional method by which TM cells can communicate with each other.

Our live-imaging of actin dynamics in human TM cells provide additional insight into the function of the actin cytoskeleton in TM cells. Only one other study has investigated actin dynamics in real-time using live porcine TM cells transfected with a GFP-fused actin construct.[43] In response to Y27632 treatment, they showed that stress fibers were rapidly disassembled and there was a major change in cell shape, similar to that described in this study. F-actin–labeled punctate vesicles were detected, but were not as numerous as in our study. This is likely due to differences in actin staining methods and/or imaging resolution. The SiR-actin used in this study is a Jasplakinolide analog, which binds to F-actin with high affinity.[44] This small cell permeable fluorescent probe labels all TM cells in a field and thus has a major advantage over transfection because transfection efficiency is low for TM cells. However, there is still some debate as to whether SiR-actin stabilizes F-actin structures or induces actin polymerization because of its structural similarities to Jasplakinolide.[45] Despite this, we found several differences in the actin labeling in control, and CK-666– and Y27632-treated TM cells. Stress fibers appeared thicker and there were fewer, less dynamic actin-positive vesicles when TM cells were treated with the filopodia inhibitor, CK-666. Conversely, few stress fibers were detected and the punctate vesicles were more dynamic and moved all over the cell when TM cells were treated with the Rho kinases inhibitor, Y27632. Thus, using SiR-actin to monitor actin dynamics in live human

TM cells may be a valuable tool to evaluate the effects of drugs on the actin cytoskeleton.

Here, we showed transfer of mitochondria between TM cells. Studies in other cell types showed mitochondrial transfer via TNTs connecting cells of different types can rescue stressed cells from apoptosis.[24,27] Although the functional significance of mitochondrial transfer in TM cells has yet to be determined, the transfer of mitochondria may help maintain the health of the TM tissue. It should be noted that glaucomatous TM has elevated levels of reactive oxygen species (ROS), which impairs mitochondrial function.[46] If damaged mitochondria are transferred between glaucomatous TM cells via TNTs, this could exacerbate the pathogenic process.

In conclusion, our results describe a novel cellular structure by which TM cells may directly communicate with each other. This may be especially advantageous to circumvent the limitations of diffusion-based signaling in the fluid environment of the TM. Future studies will focus on identifying molecules involved in TNT formation and the signals that are transferred via TNTs.

References

1. Dismuke WM, Challa P, Navarro I, Stamer WD, Liu Y. Human aqueous humor exosomes. *Exp Eye Res*. 2015;132:73–77.

2. Junglas B, Yu AH, Welge-Lussen U, Tamm ER, Fuchshofer R. Connective tissue growth factor induces extracellular matrix deposition in human trabecular meshwork cells. *Exp Eye Res*. 2009;88:1065–1075.

3. Mao W, Millar JC, Wang WH, et al. Existence of the canonical Wnt signaling pathway in the human trabecular meshwork. *Invest Ophthalmol Vis Sci*. 2012;53:7043–7051.

4. Wordinger RJ, Sharma T, Clark AF. The role of TGF-beta2 and bone morphogenetic proteins in the trabecular meshwork and glaucoma. *J Ocul Pharmacol Ther*. 2014;30:154–162.

5. Kelley MJ, Rose AY, Song K, et al. Synergism of TNF and IL-1 in the induction of matrix metalloproteinase-3 in trabecular meshwork. *Invest Ophthalmol Vis Sci*. 2007;48:2634–2643.

6. Acott TS, Samples JR, Bradley JM, Bacon DR, Bylsma SS, Van Buskirk EM. Trabecular repopulation by anterior trabecular meshwork cells after laser trabeculoplasty. *Am J Ophthalmol*. 1989;107:1–6.

7. Kelley MJ, Rose AY, Keller KE, Hessle H, Samples JR, Acott TS. Stem cells in the trabecular meshwork: present and future promises. *Exp Eye Res*. 2009;88:747–751.

8. Muller P, Rogers KW, Yu SR, Brand M, Schier AF. Morphogen transport. *Development*. 2013;140:1621–1638.

9. Entchev EV, Schwabedissen A, Gonzalez-Gaitan M. Gradient formation of the TGF-beta homolog Dpp. *Cell*. 2000;103:981–991.

10. Tojkander S, Gateva G, Lappalainen P. Actin stress fibers–assembly, dynamics and biological roles. *J Cell Sci*. 2012;125:1855–1864.

11. Mattila PK, Lappalainen P. Filopodia: molecular architecture and cellular functions. *Nat Rev Mol Cell Biol*. 2008;9:446–454.

12. Nobes CD, Hall A. Rho, rac and cdc42 GTPases: regulators of actin structures, cell adhesion and motility. *Biochem Soc Trans*. 1995;23:456–459.

13. Inoue T, Tanihara H. Rho-associated kinase inhibitors: a novel glaucoma therapy. *Prog Retin Eye Res*. 2013;37:1–12.

14. Vittitow JL, Garg R, Rowlette LL, Epstein DL, O'Brien ET, Borras T. Gene transfer of dominant-negative RhoA increases outflow facility in perfused human anterior segment cultures. *Mol Vis*. 2002;8:32–44.

15. Rao PV, Pattabiraman PP, Kopczynski C. Role of the Rho GTPase/Rho kinase signaling pathway in pathogenesis and treatment of glaucoma: Bench to bedside research. *Exp Eye Res*. 2017;158:23–32.

16. Rao PV, Deng PF, Kumar J, Epstein DL. Modulation of aqueous humor outflow facility by the Rho kinase-specific inhibitor Y-27632. *Invest Ophthalmol Vis Sci*. 2001;42:1029–1037.

17. Lu Z, Overby DR, Scott PA, Freddo TF, Gong H. The mechanism of increasing outflow facility by rho-kinase inhibition with Y-27632 in bovine eyes. *Exp Eye Res*. 2008;86:271–281.

18. Tian B, Kaufman PL. Comparisons of actin filament disruptors and Rho kinase inhibitors as potential antiglaucoma medications. *Expert Rev Ophthalmol*. 2012;7:177–187.

19. Gonzalez JM, Ko MK, Pouw A, Tan JC. Tissue-based multiphoton analysis of actomyosin and structural responses in human trabecular meshwork. *Sci Rep*. 2016;6:21315.

20. Rustom A, Saffrich R, Markovic I, Walther P, Gerdes HH. Nanotubular highways for intercellular organelle transport. *Science*. 2004;303:1007–1010.

21. Sherer NM, Mothes W. Cytonemes and tunneling nanotubules in cell-cell communication and viral pathogenesis. *Trends Cell Biol*. 2008;18:414–420.

22. Davis DM, Sowinski S. Membrane nanotubes: dynamic long-distance connections between animal cells. *Nat Rev Mol Cell Biol*. 2008;9:431–436.

23. Sowinski S, Jolly C, Berninghausen O, et al. Membrane nanotubes physically connect T cells over long distances presenting a novel route for HIV-1 transmission. *Nat Cell Biol*. 2008;10:211–219.

24. Islam MN, Das SR, Emin MT, et al. Mitochondrial transfer from bone-marrow-derived stromal cells to pulmonary alveoli protects against acute lung injury. *Nat Med*. 2012;18:759–765.

25. Climent M, Quintavalle M, Miragoli M, Chen J, Condorelli G, Elia L. TGFbeta triggers miR-143/145 Transfer from smooth muscle cells to endothelial cells, thereby modulating vessel stabilization. *Circ Res*. 2015;116:1753–1764.

26. Gousset K, Schiff E, Langevin C, et al. Prions hijack tunnelling nanotubes for intercellular spread. *Nat Cell Biol*. 2009;11:328–336.

27. Liu K, Ji K, Guo L, et al. Mesenchymal stem cells rescue injured endothelial cells in an in vitro ischemia-reperfusion model via tunneling nanotube like structure-mediated mitochondrial transfer. *Microvasc Res*. 2014;92:10–18.

28. Rocca CJ, Kreymerman A, Ur SN, et al. Treatment of inherited eye defects by systemic hematopoietic stem cell transplantation. *Invest Ophthalmol Vis Sci*. 2015;56:7214–7223.

29. Chinnery HR, Pearlman E, McMenamin PG. Cutting edge: Membrane nanotubes in vivo: a feature of MHC class II+ cells in the mouse cornea. *J Immunol*. 2008;180:5779–5783.

30. Wittig D, Wang X, Walter C, Gerdes HH, Funk RH, Roehlecke C. Multi-level communication of human retinal pigment epithelial cells via tunneling nanotubes. *PLoS One*. 2012;7: e33195.

31. Stamer WD, Seftor RE, Williams SK, Samaha HA, Snyder RW. Isolation and culture of human trabecular meshwork cells by extracellular matrix digestion. *Curr Eye Res*. 1995;14:611–617.

32. Hetrick B, Han MS, Helgeson LA, Nolen BJ. Small molecules CK-666 and CK-869 inhibit actin-related protein 2/3 complex by blocking an activating conformational change. *Chem Biol*. 2013;20:701–712.

33. Lutjen-Drecoll E. Functional morphology of the trabecular meshwork in primate eyes. *Prog Retin Eye Res*. 1999;18:91–119.

34. Inomata H, Bill A, Smelser GK. Aqueous humor pathways through the trabecular meshwork and into Schlemm's canal in the cynomolgus monkey (Macaca irus). An electron microscopic study. *Am J Ophthalmol*. 1972;73:760–789.

35. Gong H, Tripathi RC, Tripathi BJ. Morphology of the aqueous outflow pathway. *Microsc Res Tech*. 1996;33:336–367.

36. Grierson I, Lee WR, Abraham S, Howes RC. Associations between the cells of the walls of Schlemm's canal. *Albrecht Von Graefes Arch Klin Exp Ophthalmol*. 1978;208:33–47.

37. Nawaz M, Fatima F. Extracellular vesicles, tunneling nanotubes, and cellular interplay: synergies and missing links. *Front Mol Biosci*. 2017;4:50.

38. Onfelt B, Nedvetzki S, Benninger RK, et al. Structurally distinct membrane nanotubes between human macrophages support long-distance vesicular traffic or surfing of bacteria. *J Immunol*. 2006;177:8476–8483.

39. Abounit S, Zurzolo C. Wiring through tunneling nanotubes–from electrical signals to organelle transfer. *J Cell Sci*. 2012; 125:1089–1098.

40. Gerdes HH, Rustom A, Wang X. Tunneling nanotubes, an emerging intercellular communication route in development. *Mech Dev*. 2013;130:381–387.

41. Bohil AB, Robertson BW, Cheney RE. Myosin-X is a molecular motor that functions in filopodia formation. *Proc Natl Acad Sci U S A*. 2006;103:12411–12416.

42. Gousset K, Marzo L, Commere PH, Zurzolo C. Myo10 is a key regulator of TNT formation in neuronal cells. *J Cell Sci*. 2013; 126:4424–4435.

43. Fujimoto T, Inoue T, Inoue-Mochita M, Tanihara H. Live cell imaging of actin dynamics in dexamethasone-treated porcine trabecular meshwork cells. *Exp Eye Res*. 2016;145:393–400.

44. Lukinavicius G, Reymond L, D'Este E, et al. Fluorogenic probes for live-cell imaging of the cytoskeleton. *Nat Methods*. 2014;11:731–733.

45. Melak M, Plessner M, Grosse R. Actin visualization at a glance. *J Cell Sci*. 2017;130:525–530.

46. Sacca SC, Pulliero A, Izzotti A. The dysfunction of the trabecular meshwork during glaucoma course. *J Cell Physiol*. 2015;230:510–525.